Evaluating Robustness to Context-Sensitive Feature Perturbations of Different Granularities

Isaac Dunn, Laura Hanu[*], Hadrien Pouget[*], Daniel Kroening, Tom Melham
University of Oxford
[*]Equal contribution
isaac.dunn@cs.ox.ac.uk

Abstract

We cannot guarantee that training datasets are representative of the distribution of inputs that will be encountered during deployment. So we must have confidence that our models do not over-rely on this assumption. To this end, we introduce a new method that identifies context-sensitive feature perturbations (e.g. shape, location, texture, colour) to the inputs of image classifiers. We produce these changes by performing small adjustments to the activation values of different layers of a trained generative neural network. Perturbing at layers earlier in the generator causes changes to coarser-grained features; perturbations further on cause finer-grained changes. Unsurprisingly, we find that state-of-the-art classifiers are not robust to any such changes. More surprisingly, when it comes to coarse-grained feature changes, we find that adversarial training against pixel-space perturbations is not just unhelpful: it is *counterproductive*.

1 Introduction

Deep learning models have proven to be powerful tools for tasks including image classification (Touvron et al. 2020; Xie et al. 2019), with the ability to automatically identify useful features of their training images and combine these to provide accurate label predictions (Olah et al. 2020). Under the assumption that data are independently and identically distributed (i.i.d.), they have shown a remarkable ability to generalise to unseen inputs (Neyshabur et al. 2017). However, it is increasingly clear that the performance of these models drops drastically without this assumption; optimising for i.i.d. accuracy alone results in models that are not robust to even modest distributional shifts (Rosenfeld, Zemel, and Tsotsos 2018; Jo and Bengio 2017; Geirhos et al. 2018; Hendrycks and Dietterich 2019). This is concerning because the non-static nature of the real world may well cause the distribution of inputs to shift during deployment, and because it is difficult for any finite training set to capture the full range of inputs that may be encountered. A model's lack of robustness likely occurs due in part to over-reliance on non-robust features that correlate well under the i.i.d. assumption but stop providing useful information after a shift (Ilyas et al. 2019). Before deploying models, especially in safety-critical contexts, we must evaluate their robustness to possible unknown shifts in the distribution of encountered inputs.

In this work, we introduce a new method that evaluates the robustness of neural networks to changes that (a) are context-sensitive perturbations to features that vary in the training data and (b) vary in granularity as we choose. By 'context-sensitive', we mean changes that are specific to the semantics of the local objects in the image, such as object shape, position, size, pose, colour and texture. By 'granularity', we mean the scope of a change in the image: a coarse-grained change affects a large region of the image, while the finest-grained change possible is to a single pixel.

Why are these two properties desirable? We ultimately want to evaluate robustness to changes that might plausibly be encountered at deployment. For a given starting image, most ℓ_p norm-constrained pixel perturbations result in an image very unlikely to be encountered at deployment; the few that are plausible are those that represent a context-sensitive change to features in a way that has been seen in the training data. For instance, a perturbation that lengthens a table by darkening a contiguous region of the image is much more interesting than almost all perturbations of a similar size to the same pixels. Furthermore, by evaluating robustness to such changes at different granularities, we can investigate whether robustness in one respect improves or worsens robustness in other respects.

We obtain context-sensitive changes to features by taking a pre-trained generative neural network and perturbing its latent activation values as it generates images. This works because the neurons at different layers of a generator encode the useful features for generating images (Bau et al. 2019). We can control the granularity of the downstream change by selecting the layers at which the activations are perturbed: perturbations to earlier layers result in coarser-grained changes (e.g., the shape of a building), while later perturbations result in finer-grained changes (e.g., the texture of a brick).

We use this method to evaluate the robustness of state-of-the-art ImageNet classifiers to context-specific feature perturbations of different granularities. Besides finding that these models are not robust in this sense, we make the surprising finding that using classifiers adversarially that were trained to be robust to bounded pixel perturbations actually *decreases* robustness to coarse-grained perturbations. This may be because such classifiers must necessarily depend

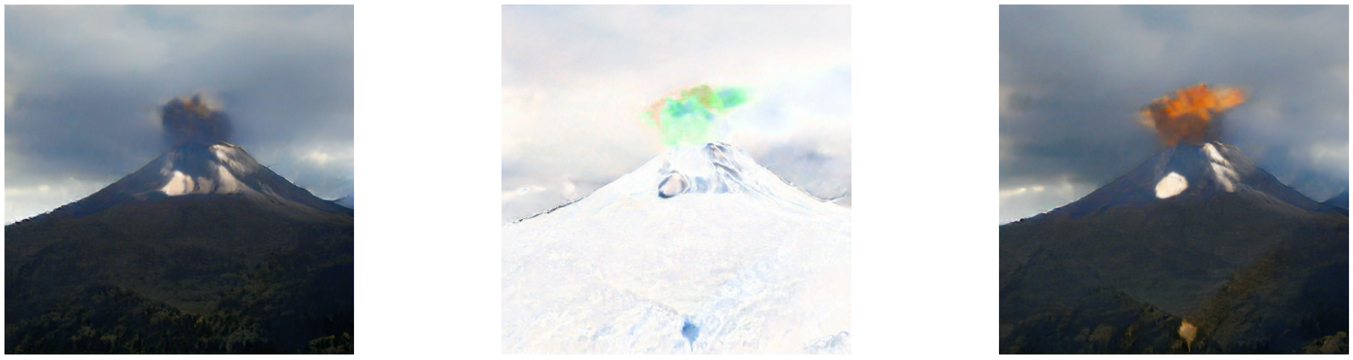
(a) Original image. (b) Difference from perturbation. (c) Perturbed image.

Figure 1: An example of changing the computed classification from ‘volcano’ to target label ‘goldfish’ using context-sensitive feature perturbations of all granularities. Coarser-grained changes include darkening the sky, causing an eruption of lava, and adding a rocky outcrop in the foreground; finer-grained changes include slightly flattening the curve of the volcano, and adjustments to the texture of the trees, rocks and cloud.

more on coarser-grained features of images than classifiers optimised for accuracy on i.i.d. inputs, which tend to rely on fine-grained features such as texture (Geirhos et al. 2019). Our results strengthen and expand upon related findings from Yin et al. (2019), who find that classifiers robust to pixel-level perturbations are less robust to corruptions of certain context-insensitive features such as artificial ‘fog’ and 2D sinusoids.

2 Background

Robustness under distributional shift When training a discriminative neural network, the goal is typically to minimise the expected loss $\mathbb{E}_{(x,y)\sim P_0}[l(x, y;\ \theta)]$ with respect to the model parameters θ, where P_0 is the training distribution over feature space $\mathbb{X}$ and labels in $\mathbb{Y}$. In real-world scenarios, however, we cannot depend on the distribution at deployment remaining identical to P_0 (i.e. we cannot rely on the i.i.d. assumption). To ensure that models behave well in practice, it is necessary to make distributionally robust models: they should perform well even after a shift to their input distribution. Studies have shown that there are many possible shifts to which classifiers are not robust, motivating a large body of literature which deals with identifying and correcting these problems (Rosenfeld, Zemel, and Tsotsos 2018; Jo and Bengio 2017; Geirhos et al. 2018; Hendrycks and Dietterich 2019; Amodei et al. 2016; Sinha, Namkoong, and Duchi 2018; He, Shen, and Cui 2019).

Generative Adversarial Networks GANs are an approach to training generative neural networks that map from a known standard probability distribution to the distribution of the training data. See a tutorial for details (Goodfellow 2017). While other types of generative networks exist, we focus on the use of GANs in this work for their crispness. Generative networks have been found to display an interesting property: different layers, and even different neurons, encode different kinds of features of the image. Earlier layers tend to encode higher-level information about objects in the image, whereas later layers deal more with “low-level materials, edges, and colours” (Bau et al. 2019, p.7). In addition, it is possible to vary features such as zoom, object position and rotation, simply by moving the input to the model in a linear walk (Jahanian, Chai, and Isola 2019).

3 Related Work

Measuring robustness This paper builds on a body of work examining trained models’ robustness to a range of changes. One approach is to apply a hand-selected range of possible corruptions such as Gaussian noise or simulated effects such as fog or motion blur. Such robustness benchmarks have been created for datasets including traffic signs (Temel et al. 2017), ImageNet (Hendrycks and Dietterich 2019), MNIST (Mu and Gilmer 2019) and Cityscapes (Michaelis et al. 2019). Snoek et al. (2019) evaluate the robustness of the calibration of classifiers’ *confidences* to rotated and translated images, as well as to out-of-distribution inputs such as not-MNIST (Bulatov 2011). Another approach is to gather new data, either replicating original dataset creation processes (Recht et al. 2019) or deliberately gathering data representing a challenging shift in distribution (Hendrycks et al. 2019); in both cases, classifiers were found to fail to generalise to the new distributions. Our paper builds on the foundations laid by these works, providing automaticity by evaluating robustness to *learnt* features that are sensitive to the local semantics.

Adversarial robustness There has been much recent work on ‘adversarial examples’: inputs deliberately crafted by an adversary to fool a model (Gilmer et al. 2018). In this literature, an attacker is modelled as having certain capabilities to construct pathological inputs, while the ‘defender’ aims to create systems that are robustly correct to all inputs within this threat model. Such attacks can be viewed as the worst-case distributional shift within the threat model. The customary threat model is constrained perturbations to the pixel values of a given image (Goodfellow, Shlens, and

Szegedy 2015), for which adversarial robustness does not imply robustness to more meaningful changes that induce large changes in pixel values. But there is a burgeoning interest in new threat models that allow *meaningful* changes to given images. While the purpose of our method is safety (to evaluate models' distributional robustness to plausible shifts in the distribution of inputs), rather than to serve as an adversarial attack for security evaluations, some existing 'semantic attacks' are related to our method.

Semantic adversarial robustness Initially, semantic adversarial examples were constructed using context-insensitive hand-coded methods that perturbed features such as colouring (Hosseini and Poovendran 2018), rotations and translations (Engstrom et al. 2019b), and corruptions such as blurring and fog (Hendrycks and Dietterich 2019) in an ad-hoc manner. Another possible approach, albeit prohibitively expensive for most domains, is to write an invertible differentiable renderer and perturb its parameters to effect semantic changes in the scene (Liu et al. 2019; Jain et al. 2019). More recently, context-sensitive methods have been proposed that use generative models to avoid the need to hand-code specific features.

Qiu et al. (2019) use a dataset labelled with various semantic features to train a generative model that allows inputs determining these features to be adversarially adjusted. Bhattad et al. (2019) utilise learnt colourisation and texture-transfer models to identify worst-case changes to the colour and texture of given images. Gowal et al. (2019) adversarially compose disentangled learned representations of different inputs. Defense-GAN (Samangouei, Kabkab, and Chellappa 2018) is not an evaluation or attack, but an attempt to mitigate attacks by projecting onto the GAN's learnt manifold. Dunn et al. (2019) train a GAN to output a distribution of images that fools the target classifier. Three imaginative papers construct semantic adversarial examples using some search procedure to identify a suitable input to a trained generative model (Zhao, Dua, and Singh 2017; Song et al. 2018; Wang et al. 2020; Alzantot et al. 2018); Wong and Kolter (2020) do likewise for a generator trained on already-perturbed data. We build on the common theme: using a generative model to learn meaningful context-specific semantic features. However, our method is the first to perturb the generator network's latent activations—not just the input. This leverages the *full* range of granularities of feature representations learnt from the training dataset, rather than just the maximally-coarse semantics encoded in the input, allowing for a much richer space of manipulations. Evidence of this richness is given in our results.

4 Method

Suppose that we have a trained, differentiable image classifier $f : \mathbb{X} \to \mathbb{R}^{|\mathbb{Y}|}$ whose robustness we would like to evaluate, where $\mathbb{X} = \mathbb{R}^{3\times w\times h}$ is RGB pixel space and $\mathbb{Y}$ is the set of class labels over which f outputs a confidence distribution. Suppose that we also have a trained generator neural network $g : \mathbb{Z} \to \mathbb{X}$, which maps from a standard Gaussian distribution over its input space $\mathbb{Z} = \mathbb{R}^m$ to the distribution of training images. Although we use the generator of a GAN, a VAE or any other generative model would be equally suitable.

Since a feedforward network is a sequence of layers, we can consider g to be a composition of functions $g = g_n \circ g_{n-1} \circ ... \circ g_1$. For instance, in our main experiments, we decompose BigGAN (Brock, Donahue, and Simonyan 2019) into its residual blocks. Here, $g_i : \mathbb{A}_{i-1} \to \mathbb{A}_i$ is the ith layer, taking activations $a_{i-1} \in \mathbb{A}_{i-1}$ from the previous layer and outputting the resulting activation tensor $g_i(a_{i-1}) \in \mathbb{A}_i$. Splitting in this way allow us to introduce a perturbation $p_i \in \mathbb{A}_i$ to layer i's activations, before continuing the forward pass through the rest of the generator. Given such a perturbation tensor $p_i \in \mathbb{A}_i$ for each layer i, we can define perturbed layer functions $g'_i(a_{i-1}) = g_i(a_{i-1}) + p_i$. By performing such perturbations at every activation space, we obtain the perturbed output of the entire generator, $g'(z;\ p_0,\ ...,\ p_n) = (g'_n \circ g'_{n-1} \circ ... \circ g'_1)(z + p_0)$.

Suppose that we have sampled some generator input z, and automatically determined the correct label y of its image under the generator when unperturbed, $g'(z;\ 0, ..., 0)$. This is best done using a conditional generator that also takes a label as input (Mirza and Osindero 2014), but can also be achieved by assuming that the classifier's initial output is correct. We now need a procedure to identify suitable perturbation tensors $\boldsymbol{p}^* = (p^*_0, ..., p^*_n) \in \mathbb{A}_0 \times \ldots \times \mathbb{A}_n$ such that the classifier's output on $g'(z;\ \boldsymbol{p}^*)$ is not y but some other label, while the true label of $g'(z;\ \boldsymbol{p}^*)$ remains y.

Ensuring misclassification We can define a loss function $\ell : \mathbb{R}^{|\mathbb{Y}|} \times \mathbb{Y} \to \mathbb{R}$ such that $\ell(f(g'(z;\ \boldsymbol{p})),\ y)$ is minimised when the classifier predicts any label but the correct y, or such that $\ell(f(g'(z;\ \boldsymbol{p})),\ t)$ is minimised when the classifier incorrectly predicts target label t. There are many possibilities, but in this paper we focus on the latter case only, using $\ell(f(x),\ t) = \max_{j\in\mathbb{Y}} f(x)_j - f(x)_t$, the variant found to be most effective by Carlini and Wagner (2017). Noting that ℓ, f and each g'_i are differentiable, we use the usual backpropagation algorithm to compute the derivative of $\ell(f(g'(z;\ \boldsymbol{p})),\ y)$ with respect to $\boldsymbol{p}$. We then use a gradient-descent optimisation over $\boldsymbol{p}$ to find a perturbation $\boldsymbol{p}^*$ that minimises ℓ. By definition of ℓ, this optimal $\boldsymbol{p}^*$ will ensure that the classifier mislabels perturbed image $g'(z;\ \boldsymbol{p}^*)$.

Ensuring the true label remains unchanged But we also need the true label of $g'(z;\ \boldsymbol{p}^*)$ to remain y, else f might in fact be predicting the correct label. Our approach is to assume that *small* changes to an image will not change its correct label (we verify this in our experiments). So we would like to identify the smallest perturbation that induces the kind of mislabelling we are investigating. The approach we take is to constrain the maximum magnitude of the perturbation—computed as the Euclidean norm of the vector obtained by 'flattening' and concatenating the perturbation tensors p_i—and gradually relaxing this constraint during optimisation until a perturbation $\boldsymbol{p}^*$ inducing the desired mislabelling is found. The quicker the constraint is relaxed, the quicker a mislabelling is found, but the larger the expected perturbation.

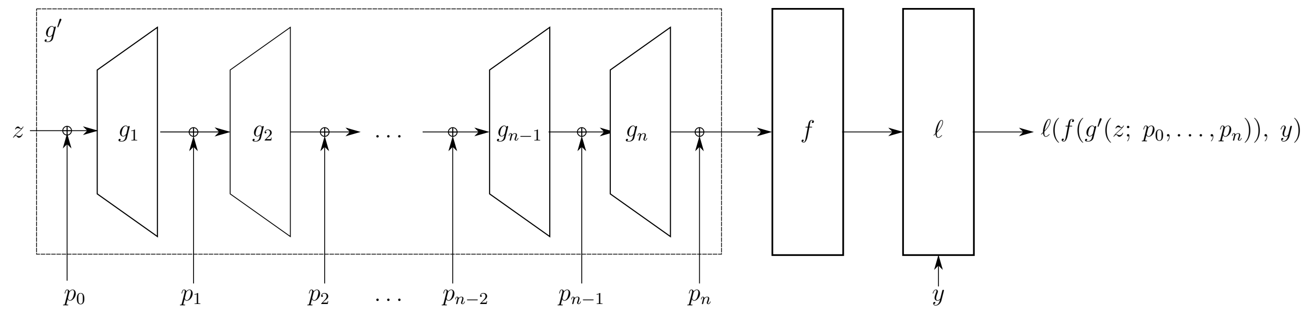

Figure 2: Illustration of a forward pass with perturbations to the latent activation values at n layers in the generator network.

Per-neuron perturbation scaling to promote uniformity The typical activation values of separate neurons differ in scale, even within a single layer. If one varies from -1 to 1, while another varies from -0.1 to 0.1, then a perturbation of magnitude 0.5 is likely to have quite different downstream effects on the image depending on which of these neurons it affects. To correct for this, we scale the perturbation for each neuron to the empirically-measured range. That is, rather than adding perturbation tensor p_i directly to the activation tensor at layer i, we add $p_i \odot \sigma_i$, where $\odot$ is element-wise multiplication and σ_i is an empirically-measured tensor of standard deviations of the activation values at layer i.

In future work, it may be desirable to further fine-tune the scale of the perturbations applied to each neuron. In the present work, however, the above scaling procedure is sufficient to normalise the downstream effect of perturbing different neurons; if it were insufficient, then too many of the perturbed images would no longer be recognisable as their original class.

5 Experimental Evaluation

In this section, we apply our method to evaluate the robustness of state-of-the-art classifiers to context-specific feature perturbations of different granularity. Primarily, we evaluate ImageNet-1K classification (Russakovsky et al. 2015), perturbing the features learnt by a pre-trained BigGAN (Brock, Donahue, and Simonyan 2019). We evaluate two standard classifiers, and two 'robust' classifiers adversarially trained against bounded pixel-space perturbations. First, the state-of-the-art on ImageNet, EfficientNet-B4 with NoisyStudent training (Xie et al. 2019). This was the highest-accuracy classifier for which pre-trained weights were available. Next, the standard ResNet50 classifier (He et al. 2016). Finally, two ResNet50 classifiers adversarially trained against pixel-space perturbations: one from Engstrom et al. (2019a) trained using an ℓ_2-norm PGD attack with radius $\epsilon = 0.3$, and another from Wong, Rice, and Kolter (2020), trained with the FGSM attack for robustness against ℓ_∞ with $\epsilon = 4/255$. See Appendix A for further details.

We focus exclusively on targeted misclassifications, for which a randomly predetermined target label $t \in \mathbb{Y}$ is chosen for each input, since failure in this case implies significant weakness. A classifier is more robust to a class of perturbations if larger-magnitude perturbations of that kind are required to induce the targeted classification. Recall that we gradually relax the constraint on the magnitude of the perturbations to activation values: by measuring the smallest magnitude for which the classifier outputs the target class t, we can build a picture of how robust the model is to the perturbations.

We cannot guarantee that the images originally produced by BigGAN would be labelled by humans as their intended class (GANs are imperfect), or that the perturbations do not change the class of the image. The risk in making visible and varied perturbations is that it becomes difficult to ensure these not change the class. To eliminate these risks, we use five independent human judges to vote on the class of the images. As in the original ImageNet labelling protocol, a majority is used to decide the label. It is also possible to avoid human labelling, by fixing a maximum perturbation magnitude—although this does introduce a trade-off between false positives and negatives. See Appendix C for details.

Our experiments proceed as follows: we randomly generate an unperturbed image of class y; we skip this image if the classifier does not predict class y to begin with. We randomly select a target t, and find a perturbation which induces this misclassification. Human labellers vote on whether the unperturbed image is truly of class y; the image is skipped if not. If the image is not skipped, the labellers who voted to keep the unperturbed image vote on whether the perturbed image is (still) of class y.

In this way, we obtain a set of correctly-classified unperturbed images paired with incorrectly-classified perturbed counterparts for which we know both the perturbation magnitude, and whether they were successful (maintained the class of the image). We then evaluate robustness by looking at how quickly the number of successful perturbations grows as we allow for larger and larger perturbation magnitudes. To evaluate robustness to changes to different feature granularities, we repeat this robustness analysis, but restrict the perturbations to affect different subsets of layers. For full details of our experiments, refer to Appendix B.

To demonstrate that our method readily generalises, we also run our experiments on a smaller scale on two further datasets. First, the much simpler (and correspondingly easier to robustly classify) MNIST dataset (LeCun, Cortes, and Burges 1999), using one classifier optimised for i.i.d. accuracy, and one adversarially trained to be robust to an ℓ_2-norm projected gradient descent attack with $\epsilon = 0.3$. Then, another high-resolution dataset: CelebA-HQ, with our method

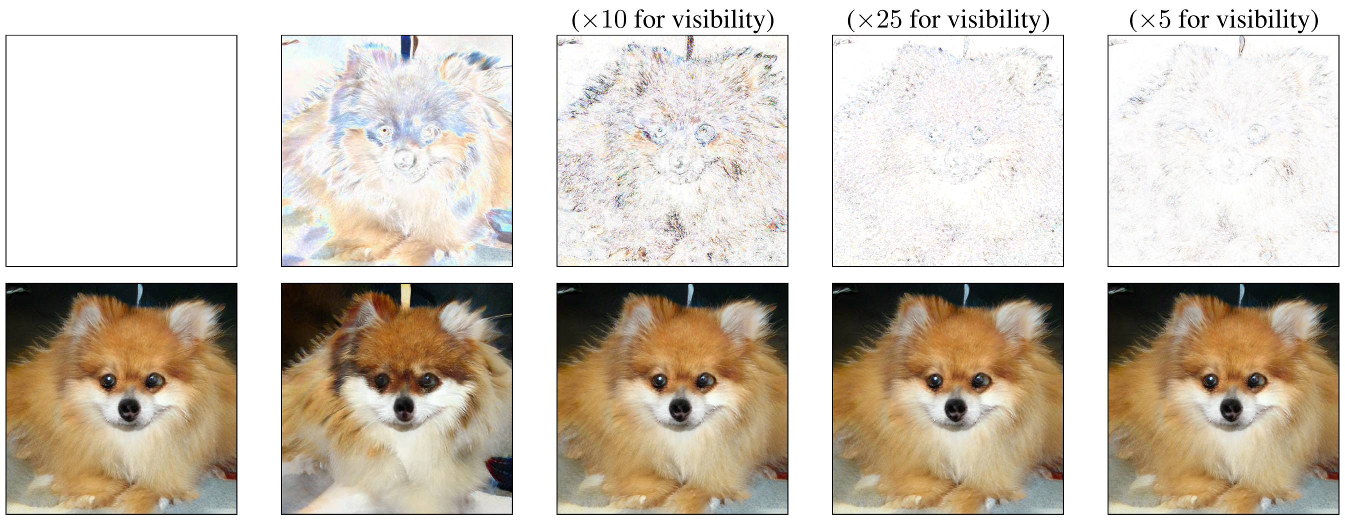

(a) Unperturbed. (b) First six layers. (c) Middle six layers. (d) Last six layers. (e) All eighteen layers.

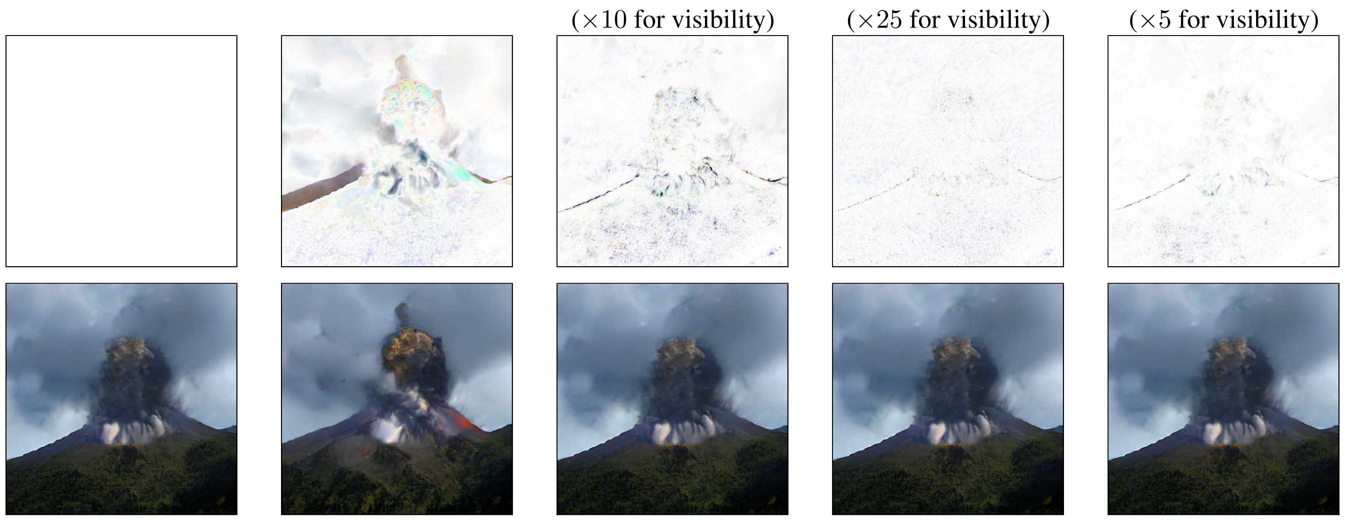

(f) Unperturbed. (g) First six layers. (h) Middle six layers. (i) Last six layers. (j) All eighteen layers.

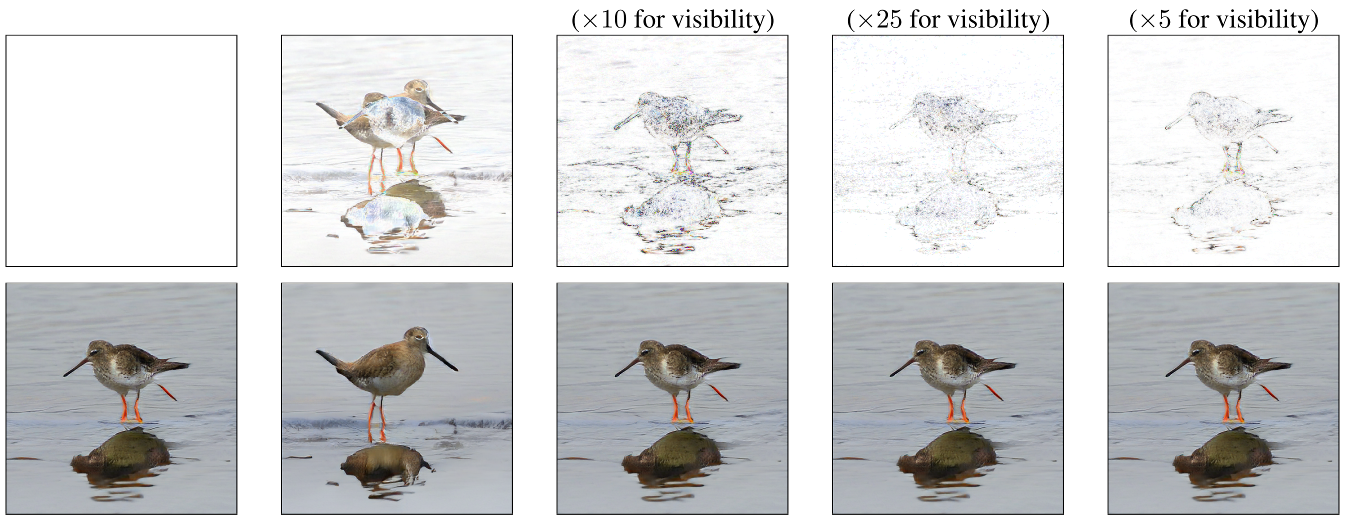

(k) Unperturbed. (l) First six layers. (m) Middle six layers. (n) Last six layers. (o) All eighteen layers.

Figure 3: Context-sensitive feature perturbations at different granularities, as controlled by perturbing activations at the generator layers indicated under each image. Differences with the unperturbed image are shown above each perturbed image. The perturbed Pomeranians (dogs) are classified as 'red king crabs', the volcanos as 'goldfish', and redshanks (birds) as 'rams'.

applied to a Progressive GAN (Karras et al. 2018).

Results

Table 1 reports the average magnitude of the misclassification-inducing perturbations. Figure 4 elaborates on this, plotting the relationships between perturbation magnitude and the cumulative proportion of inputs for which this magnitude (or smaller) is sufficient to cause the classifier to predict the target label. For each type of perturbation, for each classifier, 192 ± 20 (minimum 158) unperturbed images were labelled by the human judges, of which 53 ± 8 (max 69) images were rejected by the majority for not matching the intended label. Note that this latter quantity depends only on the pre-trained generator, not our method. See above and Appendix B for full details of our procedure.

Of course, even state-of-the-art GANs generate images that are not photorealistic. But we note that photorealism from the generative model is not necessary for our method. We want to trust our classifiers to behave correctly on images that are unambiguously of a certain class: all that is necessary is that the generated images have this property. Our standard for labelling is a majority vote among our five judges; all images that meet this criterion yet are misclassified by a model are weaknesses of the model.

Discussion of Results

Qualitative results The results in Figure 3 and Appendix D demonstrate a range of the context-specific feature perturbations that our method produces, and shows that perturbations at different layers produce downstream changes of different granularities. We are publishing the full dataset of perturbed images used in our experiments; see Appendix D.

None of the classifiers are robust to any granularity of perturbation Figure 6a shows that for all four classifiers, our method finds misclassification-inducing perturbations for over 80% of the initial generated images, even with relatively small perturbation magnitudes. This result is consistent with the notion that trained classifiers have learnt to rely on spurious (or at least fragile) feature correlations that may not generalise beyond the training regime. For instance, relying on background colour to identify the foreground object may work well if this correlation holds—as it would both during normal i.i.d. training and adversarial training—but this should not be relied upon at deployment.

Different generator layers encode meaningfully-different features Since the results show that the classifiers behave significantly differently when perturbations are restricted to different groups of layers, the kinds of features being changed must meaningfully differ. This is clear evidence that perturbing intermediate activations offers a much richer feature space than perturbing (say) the generator input only.

Pixel-space robustness improves robustness to finer-grained perturbations The lower average magnitudes required for the pixel-robust classifiers when perturbing the final six layers, as seen in the last column of Table 1 and the correspondingly flatter curves in Figure 6d, demonstrate that adversarial training generalises somewhat to confer robustness to fine-grained feature perturbations. The slightly gentler gradient at the beginning of Figure 6c suggests that this even provides some limited robustness to small perturbations of medium granularity. In both cases, this may be because the changes fall within or nearby the pixel-space ℓ_p-norm ball that the classifier is trained to be robust within.

Table 1: Mean magnitudes of misclassification-inducing perturbations, for different classifiers (rows) and different layers in the generator at which activations are perturbed (columns). Compare results within each column to compare robustness to the same granularity of perturbation.

	All layers	First 6	Middle 6	Last 6
Engstrom	36	33	21	141
“Fast”	35	29	22	102
EfficientNet	36	97	22	24
ResNet50	4.2	89	4.2	7.4

But robustness to pixel-space perturbations is a double-edged sword Perturbations to activations in the early layers of a generator induce context-sensitive, coarse-grained changes to the features of an image. These have a large magnitude when measured in pixel space, so it is unsurprising that classifiers trained to be robust to norm-constrained pixel perturbations do not have improved robustness to such feature perturbations. More surprisingly, Figure 6b and Table 1 show that pixel-space robustness in fact considerably *worsens* robustness to the coarse-grained features encoded in the first six generator layers. This may be because non-robust standard classifiers ordinarily depend mainly on fine-grained features such as texture (Geirhos et al. 2019). Conversely, pixel-space robust classifiers have been trained to ignore these fine-grained features, and so depend instead on coarse-grained features. But they can still rely on fragile correlations in the coarse-grained features, so their robustness to context-sensitive coarse-grained feature perturbations is decreased.

There is already some evidence that classifiers optimised for robustness to constrained adversarial pixel perturbations seem to have decreased robustness to corruptions concentrated in the low-frequency Fourier domain (Yin et al. 2019), decreased robustness to invariance-based attacks that change the true label but maintain the model’s prediction (Tramèr et al. 2020) and little robustness to various context-insensitive corruptions not encountered at training time (Kang et al. 2019). Our finding that such models also have significantly decreased robustness to coarse-grained context-sensitive feature perturbations strengthens and generalises these results.

MNIST The simplicity of the MNIST classification task suggests that constructing a robust classifier for MNIST should be significantly easier than for ImageNet. We find that adversarial training against pixel perturbations does not improve robustness to coarse-grained perturbations on MNIST,

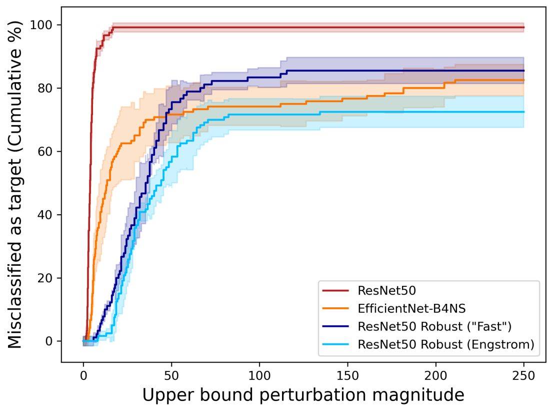

(a) Activation values perturbed at all BigGAN layers.

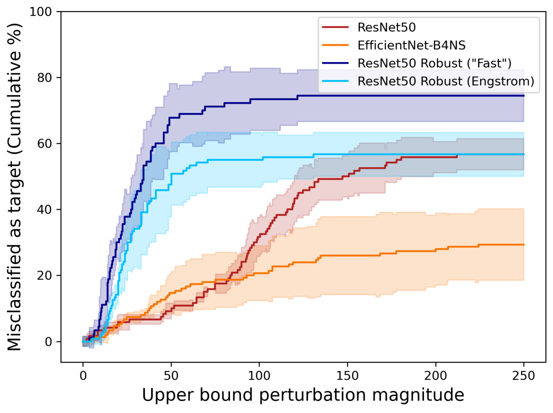

(b) Activation values perturbed in the first six layers only.

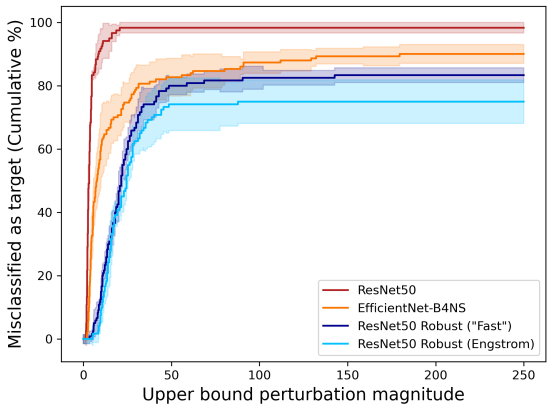

(c) Activations perturbed in the middle six layers only.

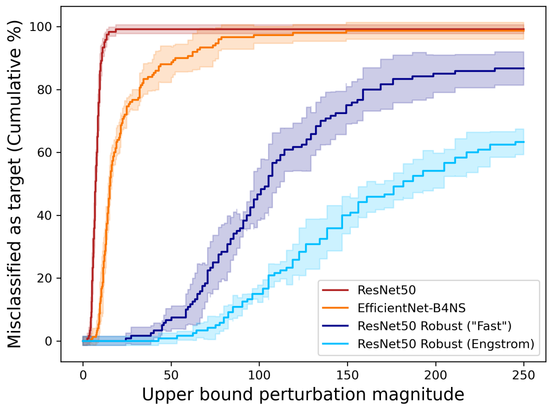

(d) Activation values perturbed in the last six layers only.

Figure 4: Graphs showing how the cumulative proportion of perturbations that induce the targeted misclassification increases with maximum perturbation magnitude. The steeper the line, the less robust the classifier to that perturbation type. The lines and translucent areas shown are the means and standard deviations between several experiments of 30 images each.

but neither does it worsen it. This is likely because the simplicity and low resolution of the dataset significantly reduces the range of possible granularities, relative to ImageNet. See Appendix F for results and discussion.

CelebA-HQ In Appendix E, we show that our method also easily generalises to work for a pre-trained Progressive GAN (Karras et al. 2018) on the CelebA-HQ dataset. This neatly demonstrates that our method is general, in that it does not depend on properties of any dataset or model.

Note that the results on ImageNet, CelebA-HQ, and MNIST show that the method described in Section 4 is sufficient. On all three we did *no* hyper-parameter tuning. We used the obvious choice for where to make perturbations, and did not tune size of the perturbations at each neuron.

6 Conclusion

Since the i.i.d. assumption cannot be relied upon during deployment, it is necessary for our models to remain performant when given inputs different from those in its training distribution. In this paper, we have introduced a new method that evaluates robustness of image classifiers to a rich class of such inputs: by dynamically perturbing the intermediate activation values of trained generative neural networks we produce context-sensitive perturbations to meaningful learnt features of different granularities. This allows evaluation of robustness to changes varying from coarse-grained properties such as object shape and colour (encoded in earlier layers) to fine-grained edges and textures (encoded in later layers).

Perhaps unsurprisingly, we find that modern state-of-the-art ImageNet classifiers are not robust to context-sensitive features perturbations at any granularity. More surprisingly, while classifiers optimised for robustness to ℓ_p norm-bounded pixel perturbations are indeed more robust to fine-grained feature perturbations, this is to the detriment of their robustness to coarse-grained feature perturbations. Besides the obvious need for improved models, our findings motivate the need for a deeper understanding of robustness of different kinds, and more comprehensive meaningful evaluations of models. We hope that the present work is a step in the right direction.

Ethics Statement

Our method produces context-dependent feature perturbations of different granularities. We hope that this line of work will eventually produce tools that can be used to thoroughly evaluate the robustness of machine learning systems. This would be extremely useful: we should only give such systems responsibility when we are sure that we can rely on them to behave well even if they are presented with inputs that do not exactly match the kind they were trained on—an inevitability in our ever-changing world.

But we should point out that although our method is a very helpful step towards a thorough robustness evaluation, it is currently insufficient. GANs are known to 'drop modes', meaning that not all kinds of variation present in the training data are learnt. Moreover, it certainly is not clear that all kinds of variation to which we desire robustness can even in principle be represented as perturbations to the intermediate activations of a generator. Therefore, our method must be viewed as one tool in a box of evaluation methods, and as an invaluable step towards more comprehensive evaluations; it must not be relied on by itself. We note also that even a thorough robustness evaluation would be insufficient, since there may be other necessary properties of models such as maintaining privacy or fairness.

Generative modelling is well-known to be dual-use, in the sense that generative models can be used for harmful as well as beneficial purposes. For example, they can be used to generate 'deepfake' videos that can deceive the viewer into thinking something untrue on an important subject (Guera and Delp 2018). Our work is not an advancement in generative modelling. Nor is it the first to identify that different intermediate neurons control different meaningful features of outputs (Bau et al. 2019). But this paper may draw more attention to this true fact, which may be helpful to malicious individuals creating harmful 'deepfake' videos. Given the importance of understanding and mitigating robustness weaknesses in deep learning models, we believe that the benefits of our work easily outweigh the costs.

In this paper, we find that robustness in the sense that most contemporary work focuses on—that is, robustness to ℓ_p norm-constrained pixel-space perturbations—is not only insufficient for robustness against high-level meaningful changes of the kind that might be encountered during deployment, but in fact *worsens* such robustness. It is important that the research community and especially organisations deploying commercial deep learning applications take note. General robustness is currently poorly understood, and very far from being achieved in practice. We hope that our work leads to more work in this area, and to more caution.

References

Alzantot, M.; Sharma, Y.; Elgohary, A.; Ho, B.-J.; Srivastava, M. B.; and Chang, K.-W. 2018. Generating Natural Language Adversarial Examples. In *Proc. 2018 Conf. Empir. Methods Nat. Lang. Process. Brussels, Belgium, Oct. 31 - Novemb. 4, 2018*, 2890–2896. Association for Computational Linguistics. ISBN 978-1-948087-84-1.

Amodei, D.; Olah, C.; Steinhardt, J.; Christiano, P. F.; Schulman, J.; and Mané, D. 2016. Concrete Problems in AI Safety. *CoRR* abs/1606.06565.

Bau, D.; Zhu, J.-Y.; Strobelt, H.; Zhou, B.; Tenenbaum, J. B.; Freeman, W. T.; and Torralba, A. 2019. GAN Dissection: Visualizing and Understanding Generative Adversarial Networks. In *ICLR 2019*. OpenReview.net.

Bhattad, A.; Chong, M. J.; Liang, K.; Li, B.; and Forsyth, D. A. 2019. Big but Imperceptible Adversarial Perturbations via Semantic Manipulation. *arXiv:1904.06347 [cs]* .

Brock, A.; Donahue, J.; and Simonyan, K. 2019. Large Scale GAN Training for High Fidelity Natural Image Synthesis. In *International Conference on Learning Representations (ICLR)*.

Bulatov, Y. 2011. Machine Learning, Etc: notMNIST Dataset.

Carlini, N.; and Wagner, D. A. 2017. Towards Evaluating the Robustness of Neural Networks. In *2017 IEEE Symposium on Security and Privacy, SP 2017, San Jose, CA, USA, May 22-26, 2017*, 39–57. IEEE Computer Society. doi:10.1109/SP.2017.49.

DeepMind. 2019. Biggan Deep 512 |.

Ding, G. W.; Wang, L.; and Jin, X. 2019. AdverTorch v0.1: An Adversarial Robustness Toolbox based on PyTorch. *arXiv preprint arXiv:1902.07623* .

Dunn, I.; Pouget, H.; Melham, T.; and Kroening, D. 2019. Adaptive Generation of Unrestricted Adversarial Inputs. *CoRR* abs/1905.02463.

Engstrom, L.; Ilyas, A.; Santurkar, S.; and Tsipras, D. 2019a. Robustness (Python Library).

Engstrom, L.; Tran, B.; Tsipras, D.; Schmidt, L.; and Madry, A. 2019b. Exploring the Landscape of Spatial Robustness. In *ICML 2019*, volume 97 of *Proceedings of Machine Learning Research*, 1802–1811. PMLR.

Geirhos, R.; Rubisch, P.; Michaelis, C.; Bethge, M.; Wichmann, F. A.; and Brendel, W. 2019. ImageNet-Trained CNNs Are Biased towards Texture; Increasing Shape Bias Improves Accuracy and Robustness. In *ICLR 2019*. OpenReview.net.

Geirhos, R.; Temme, C. R. M.; Rauber, J.; Schütt, H. H.; Bethge, M.; and Wichmann, F. A. 2018. Generalisation in humans and deep neural networks. In *NeurIPS 2018*.

Gilmer, J.; Adams, R. P.; Goodfellow, I. J.; Andersen, D.; and Dahl, G. E. 2018. Motivating the Rules of the Game for Adversarial Example Research. *CoRR* abs/1807.0.

Goodfellow, I. J. 2017. NIPS 2016 Tutorial: Generative Adversarial Networks. *CoRR* abs/1701.0.

Goodfellow, I. J.; Shlens, J.; and Szegedy, C. 2015. Explaining and Harnessing Adversarial Examples. In *ICLR 2015*.

Gowal, S.; Qin, C.; Huang, P.; Cemgil, T.; Dvijotham, K.; Mann, T. A.; and Kohli, P. 2019. Achieving Robustness in the Wild via Adversarial Mixing with Disentangled Representations. *CoRR* abs/1912.03192.

Guera, D.; and Delp, E. J. 2018. Deepfake Video Detection Using Recurrent Neural Networks. In *AVSS 2018*. IEEE. doi:10.1109/AVSS.2018.8639163.

He, K.; Zhang, X.; Ren, S.; and Sun, J. 2016. Deep Residual Learning for Image Recognition. In *CVPR 2016*, 770–778. IEEE Computer Society. doi:10.1109/CVPR.2016.90.

He, Y.; Shen, Z.; and Cui, P. 2019. NICO: A Dataset Towards Non-I.I.D. Image Classification. *CoRR* abs/1906.02899.

Hendrycks, D.; and Dietterich, T. G. 2019. Benchmarking Neural Network Robustness to Common Corruptions and Perturbations. In *ICLR 2019*. OpenReview.net.

Hendrycks, D.; Zhao, K.; Basart, S.; Steinhardt, J.; and Song, D. 2019. Natural Adversarial Examples. *CoRR* abs/1907.07174.

Hosseini, H.; and Poovendran, R. 2018. Semantic Adversarial Examples. In *CVPR Workshops 2018*, 1614–1619. IEEE Computer Society. doi:10.1109/CVPRW.2018.00212.

Ilyas, A.; Santurkar, S.; Tsipras, D.; Engstrom, L.; Tran, B.; and Madry, A. 2019. Adversarial Examples Are Not Bugs, They Are Features. In *NeurIPS 2019*.

Jahanian, A.; Chai, L.; and Isola, P. 2019. On the "steerability" of generative adversarial networks. *CoRR* abs/1907.07171.

Jain, L.; Wu, W.; Chen, S.; Jang, U.; Chandrasekaran, V.; Seshia, S. A.; and Jha, S. 2019. Generating Semantic Adversarial Examples with Differentiable Rendering. *CoRR* abs/1910.00727.

Jo, J.; and Bengio, Y. 2017. Measuring the tendency of CNNs to Learn Surface Statistical Regularities. *CoRR* abs/1711.11561.

Kang, D.; Sun, Y.; Hendrycks, D.; Brown, T.; and Steinhardt, J. 2019. Testing Robustness Against Unforeseen Adversaries. *arXiv:1908.08016 [cs, stat]* .

Karras, T.; Aila, T.; Laine, S.; and Lehtinen, J. 2018. Progressive Growing of GANs for Improved Quality, Stability, and Variation. In *ICLR 2018*.

Kingma, D. P.; and Ba, J. 2015. Adam: A Method for Stochastic Optimization. In *ICLR 2015*.

LeCun, Y.; Cortes, C.; and Burges, C. 1999. MNIST Handwritten Digit Database .

Liu, H. D.; Tao, M.; Li, C.; Nowrouzezahrai, D.; and Jacobson, A. 2019. Beyond Pixel Norm-Balls: Parametric Adversaries using an Analytically Differentiable Renderer. In *ICLR 2019*. OpenReview.net.

Melas-Kyriazi, L. 2020. lukemelas/EfficientNet-PyTorch. Original-date: 2019-05-30T05:24:11Z.

Michaelis, C.; Mitzkus, B.; Geirhos, R.; Rusak, E.; Bringmann, O.; Ecker, A. S.; Bethge, M.; and Brendel, W. 2019. Benchmarking Robustness in Object Detection: Autonomous Driving When Winter Is Coming. *CoRR* abs/1907.07484.

Mirza, M.; and Osindero, S. 2014. Conditional Generative Adversarial Nets. *CoRR* abs/1411.1.

Mu, N.; and Gilmer, J. 2019. MNIST-C: A Robustness Benchmark for Computer Vision. *CoRR* abs/1906.02337.

Neyshabur, B.; Bhojanapalli, S.; McAllester, D.; and Srebro, N. 2017. Exploring Generalization in Deep Learning. In *NIPS 2017*, 5947–5956.

Olah, C.; Cammarata, N.; Schubert, L.; Goh, G.; Petrov, M.; and Carter, S. 2020. Zoom In: An Introduction to Circuits. *Distill* doi:10.23915/distill.00024.001. Https://distill.pub/2020/circuits/zoom-in.

Qiu, H.; Xiao, C.; Yang, L.; Yan, X.; Lee, H.; and Li, B. 2019. SemanticAdv: Generating Adversarial Examples via Attribute-Conditional Image Editing. *arXiv:1906.07927 [cs, eess]* .

Radford, A.; Metz, L.; and Chintala, S. 2016. Unsupervised Representation Learning with Deep Convolutional Generative Adversarial Networks. In *ICLR 2016*.

Recht, B.; Roelofs, R.; Schmidt, L.; and Shankar, V. 2019. Do ImageNet Classifiers Generalize to ImageNet? In *ICML 2019*, volume 97 of *Proceedings of Machine Learning Research*, 5389–5400. PMLR.

Rosenfeld, A.; Zemel, R. S.; and Tsotsos, J. K. 2018. The Elephant in the Room. *CoRR* abs/1808.03305.

Russakovsky, O.; Deng, J.; Su, H.; Krause, J.; Satheesh, S.; Ma, S.; Huang, Z.; Karpathy, A.; Khosla, A.; Bernstein, M. S.; Berg, A. C.; and Li, F.-F. 2015. ImageNet Large Scale Visual Recognition Challenge. *International Journal of Computer Vision* 115(3): 211–252.

Samangouei, P.; Kabkab, M.; and Chellappa, R. 2018. Defense-GAN: Protecting Classifiers Against Adversarial Attacks Using Generative Models. In *ICLR 2018*.

Sinha, A.; Namkoong, H.; and Duchi, J. C. 2018. Certifying Some Distributional Robustness with Principled Adversarial Training. In *ICLR 2018*. OpenReview.net.

Snoek, J.; Ovadia, Y.; Fertig, E.; Lakshminarayanan, B.; Nowozin, S.; Sculley, D.; Dillon, J. V.; Ren, J.; and Nado, Z. 2019. Can You Trust Your Model's Uncertainty? Evaluating Predictive Uncertainty under Dataset Shift. In *NeurIPS 2019*, 13969–13980.

Song, Y.; Shu, R.; Kushman, N.; and Ermon, S. 2018. Constructing Unrestricted Adversarial Examples with Generative Models. In *NeurIPS 2018*, 8322–8333.

Tan, M.; and Le, Q. V. 2019. EfficientNet: Rethinking Model Scaling for Convolutional Neural Networks. In *ICML 2019*, volume 97 of *Proceedings of Machine Learning Research*, 6105–6114. PMLR.

Temel, D.; Kwon, G.; Prabhushankar, M.; and AlRegib, G. 2017. CURE-TSR: Challenging Unreal and Real Environments for Traffic Sign Recognition. *CoRR* abs/1712.02463.

Touvron, H.; Vedaldi, A.; Douze, M.; and Jégou, H. 2020. Fixing the train-test resolution discrepancy: FixEfficientNet. *CoRR* abs/2003.08237.

Tramèr, F.; Behrmann, J.; Carlini, N.; Papernot, N.; and Jacobsen, J. 2020. Fundamental Tradeoffs between Invariance and Sensitivity to Adversarial Perturbations. *CoRR* abs/2002.04599.

Wang, S.; Chen, S.; Chen, T.; Nepal, S.; Rudolph, C.; and Grobler, M. 2020. Generating Semantic Adversarial Examples via Feature Manipulation. *arXiv:2001.02297 [cs, stat]* .

Wong, E.; and Kolter, J. Z. 2020. Learning perturbation sets for robust machine learning. *CoRR* abs/2007.08450.

Wong, E.; Rice, L.; and Kolter, J. Z. 2020. Fast is better than free: Revisiting adversarial training. In *ICLR 2020*. OpenReview.net.

Xie, Q.; Hovy, E. H.; Luong, M.; and Le, Q. V. 2019. Self-training with Noisy Student improves ImageNet classification. *CoRR* abs/1911.04252.

Yin, D.; Lopes, R. G.; Shlens, J.; Cubuk, E. D.; and Gilmer, J. 2019. A Fourier Perspective on Model Robustness in Computer Vision. In *NeurIPS 2019*.

Zhao, Z.; Dua, D.; and Singh, S. 2017. Generating Natural Adversarial Examples. *arXiv:1710.11342 [cs]* .

A Model details

BigGAN

We use the BigGAN-deep generator architecture at the 512×512 resolution, which can be found in Table 9 of Appendix B in the paper introducing BigGAN (Brock, Donahue, and Simonyan 2019). Conveniently, this table clearly indicates the locations at which we perturb the activations; every horizontal line of the table is a point at which our method can perturb the activation values. Please refer to Appendix B of the BigGAN paper for detailed descriptions, in particular of the ResBlocks which comprise the majority of the network. Note that we in essence perform perturbations after each ResBlock; if desired, perturbations could also be performed within each block. We take the pre-trained generator published by DeepMind (DeepMind 2019).

Standard classifiers

We use two classifiers trained as usual to maximise accuracy on the training distribution. The first is from the state-of-the-art EfficientNet family (Tan and Le 2019), enhanced using noisy student training (Xie et al. 2019). We use the best readily available model and pre-trained weights for Pytorch, EfficientNet-B4 (Noisy Student) from Melas-Kyriazi (2020). The second is PyTorch's pre-trained ResNet50 (He et al. 2016), made available through the `torchvision` package of PyTorch. These classifiers' ImageNet accuracies are reported in Table 2.

Table 2: Classifiers' accuracy on ImageNet, in %

Classifier	Top-1	Top-5
ResNet50	76.15	92.87
EfficientNet-B4 NS	85.16	97.47

Robust classifiers

We use two pre-trained ResNet50 classifiers adversarially trained against bounded pixel perturbations. The first, 'ResNet50 Robust (Engstrom)', from Engstrom et al. (2019a), was trained using l_2-norm projected gradient descent attack with $\epsilon = 0.3$. The second, 'ResNet50 Robust ("Fast")', from *Fast Is Better Than Free: Revisiting Adversarial Training* (Wong, Rice, and Kolter 2020), was trained with the fast gradient sign method attack for robustness against l_∞ with $\epsilon = 4/255$. The classifiers' ImageNet accuracies and robustness to relevant attacks are shown in Table 3.

B Experimental setup

Technical details

For our experiments, we used used the neural networks described in Appendix A, and searched for context-sensitive perturbations using the procedure described in Sections 4 and 5. However, those sections did not describe the optimisation procedure used. We used the Adam optimiser (Kingma and Ba 2015) with a learning rate of 0.03 and the default β hyperparameters of 0.9 and 0.999. After each optimisation

Table 3: Classifiers' accuracy on ImageNet, and robustness to attacks, in %

Classifier	Top-1 (no attack)	Top-1 (l_2 attack $\epsilon = 0.3$)	Top-1 (l_∞ attack $\epsilon = 4/255$)
ResNet50 Robust (Engstrom)	57.90	35.16	
ResNet50 Robust ("Fast")	55.45		30.28

step, we constrained the magnitude of the perturbation by finding the L_2 norm of the perturbation 'vector' obtained by concatenating the scalars used to perturb each individual activation value, then rescaling it to have a norm no greater than our constraint. This constraint was initially set to be magnitude 1, and was slightly relaxed after each optimisation step by multiplication by 1.03 and addition of 0.1. These values were empirically found—using small amount of manual experimentation—to be a reasonable tradeoff between starting small and increasing slowly enough to find decently small perturbations, while also using a reasonable amount of compute. Typically, finding a perturbation under this regime takes $O(100)$ steps, which took $O(1 \text{ minute})$ using the single NVIDIA Tesla V100 GPU we used.

Data collection

To run our ImageNet experiments, we began by randomly sampling (y, z, t) tuples, where y is the desired true image label, z is the latent input to the generator, and t is the target label for the perturbed misclassification. For each classifier, and each kind of perturbation, we calculated perturbations based on each of these tuples. That is, with generator g, we perturb the original image $g(z; y)$ to be classified as t. These same tuples were used for all of the experiments, although the number of such tuples in each experiment varies slightly, and can be seen in Table 4.

The images then go through two filters, and they are not used if they fail to meet the requirements. Firstly, the classifier's prediction must be y, the label that was used to produce the image. If not, then the classifier is already incorrect, and so it is not worth perturbing the image to cause a misclassification. Secondly, human labellers vote whether the original image was actually of class y (this because generators are not perfect, and so may fail at making an image of the intended class). A majority vote is used, and images which are voted to not be of the intended class are discarded. The majority vote is similar to that used in the original ImageNet labelling process.

Finally, human labellers are asked to determine whether the perturbed image is of the same class as the original image, i.e. if the perturbation successfully preserved the true class, while changing the classifier's predicted class. Again, this is done by a majority vote.

The solid lines in Figure 4 show the final results. Note that they do not always reach 1. This is because we consider that if a perturbation changed the true class of an image, no suitable perturbation was found.

We separate the images into several experiments of 30 images and report the mean and standard deviation over these experiments.

Table 4: For each classifier, and for each section in which we made perturbations, the number of images included in our final results (Figure 4). This number does not include examples for which the unperturbed image was judged by labellers to be of the wrong class; this number is included in parentheses.

ResNet 50			
First 6	Middle 6	Last 6	All 18
148 (61)	147 (62)	148 (61)	148 (61)

EfficientNet-B4NS			
First 6	Middle 6	Last 6	All 18
158 (54)	157 (55)	161 (52)	148 (49)

ResNet50 Robust ("Engstrom")			
First 6	Middle 6	Last 6	All 18
136 (51)	137 (50)	138 (50)	133 (55)

ResNet50 Robust ("Fast")			
First 6	Middle 6	Last 6	All 18
95 (69)	123 (43)	123 (43)	119 (39)

Labelling interface

For both the stages at which human labelling is required, we use the interface shown in Figure 5. The user first labels whether the original image is the of the intended label, and then the perturbed image. We ask the user which of the following four options is the best description of the image:

1. "This is an image of label y"
2. "This is an image of something else"
3. "It is unclear what this image shows"
4. "This is not an image of anything meaningful"

C Experiments with no human labelling

Our perturbation method, like any making large visual changes to images, has the potential to change the true class of the image. We tackled this problem by using human labellers to identify the cases in which this happens. However, it is also possible to use the standard approach of constraining the perturbation magnitude, to limit the visual change in the final image. By setting an upper bound on the perturbation magnitude, we are more constrained in the changes we

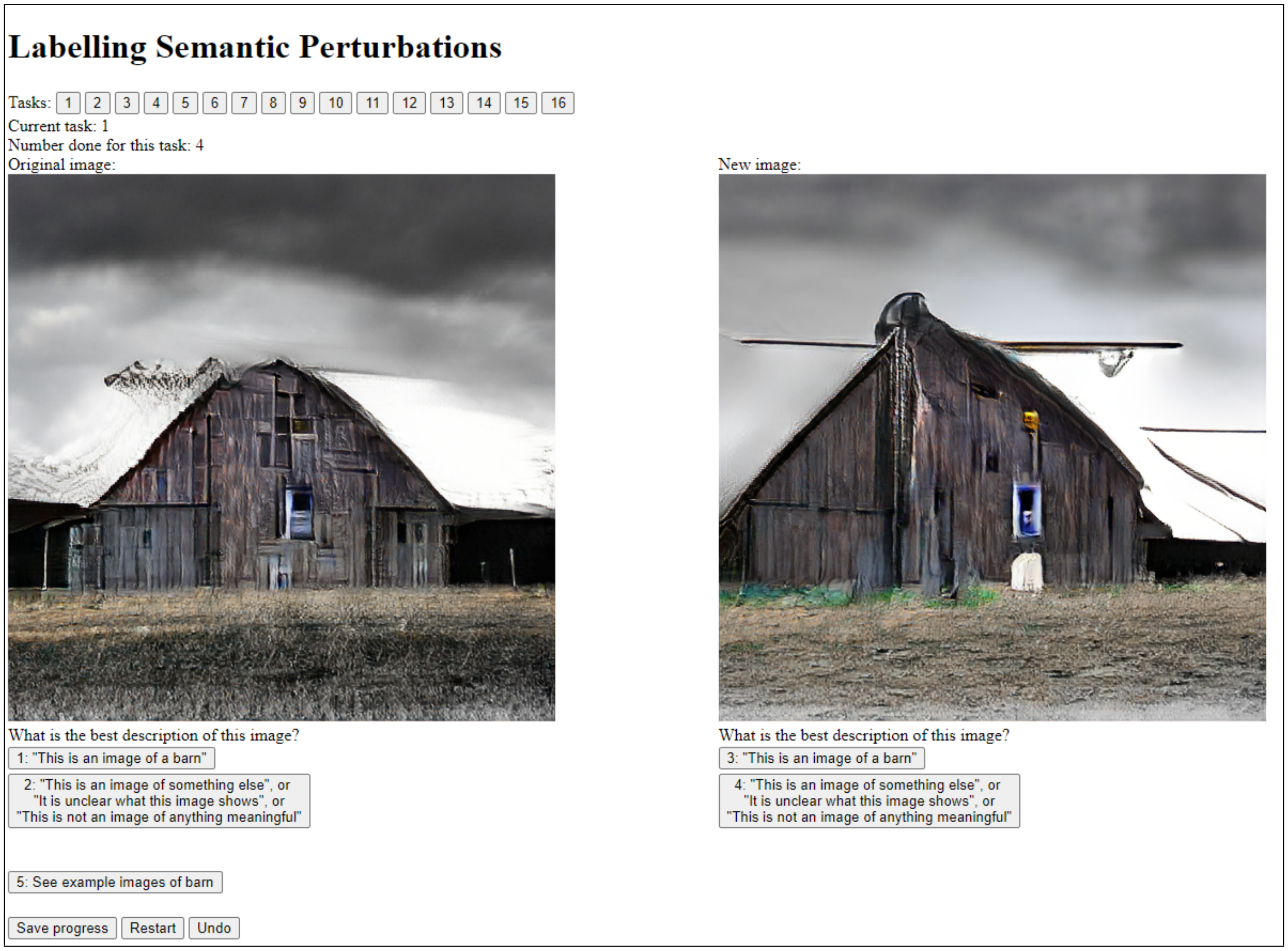
Labelling Semantic Perturbations
Tasks: 1 2 3 4 5 6 7 8 9 10 11 12 13 14 15 16
Current task: 1
Number done for this task: 4
Original image:
New image:
What is the best description of this image?
1: "This is an image of a barn"
2: "This is an image of something else", or "It is unclear what this image shows", or "This is not an image of anything meaningful"
What is the best description of this image?
3: "This is an image of a barn"
4: "This is an image of something else", or "It is unclear what this image shows", or "This is not an image of anything meaningful"
5: See example images of barn
Save progress
Restart
Undo

Figure 5: Screenshot of labelling interface. The perturbed image and buttons, on the right-hand side, are visible only when the unperturbed image (on the left) has been selected as matching the desired label. The buttons are numbered to provide keyboard shortcuts. The button at the bottom opens a web image search, in case the user is unfamiliar with the class label.

can make to images, but we also make fewer class-changing perturbations. This allows us to avoid human labelling, by accepting a small amount of error in the labels. The only way to completely avoid this error would be to make changes that *cannot* change the true class (very limiting), or have humans label the images. Figure 6 demonstrates this tradeoff for our ImageNet experiments.

D ImageNet: further examples

See Figures 7 and 8 below, which give examples of context-sensitive feature perturbations.

Please also refer to the separate Multimedia Appendix, which contains many more examples, and to the separate Data Appendix, which includes animations showing the effect of gradually introducing the perturbations to the latent activations of the generator. These give a much clearer intuition for the nature of the changes being made to the images; comparing static images alone can be difficult to interpret.

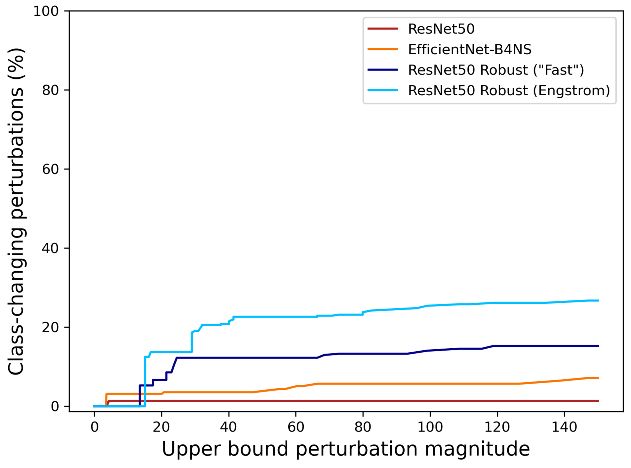

(a) Activation values perturbed at all BigGAN layers.

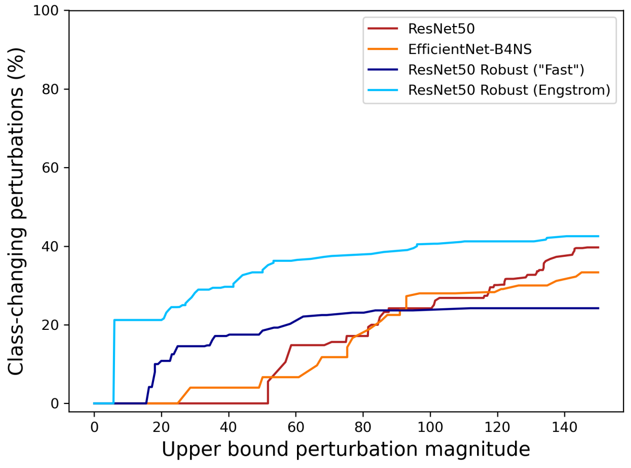

(b) Activation values perturbed in the first six layers only.

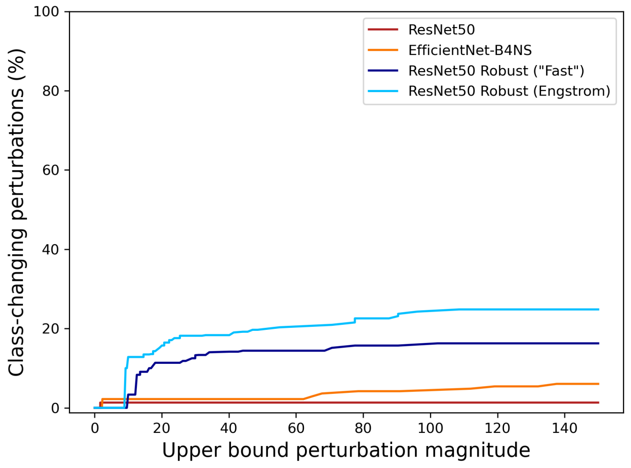

(c) Activations perturbed in the middle six layers only.

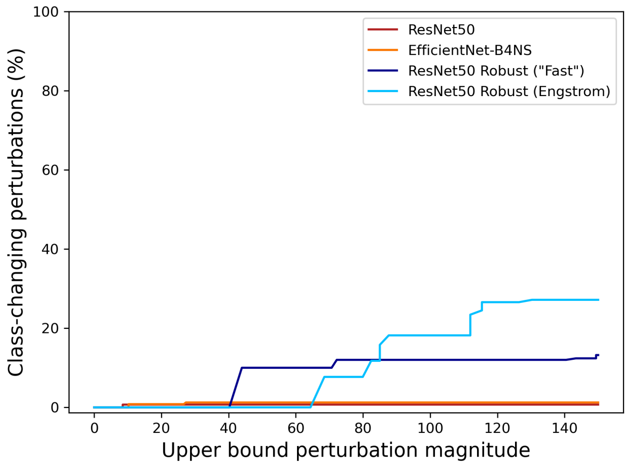

(d) Activation values perturbed in the last six layers only.

Figure 6: Number of class-changing perturbations for different upper bounds on perturbation magnitude, according to classifier, and where the perturbation is being made.

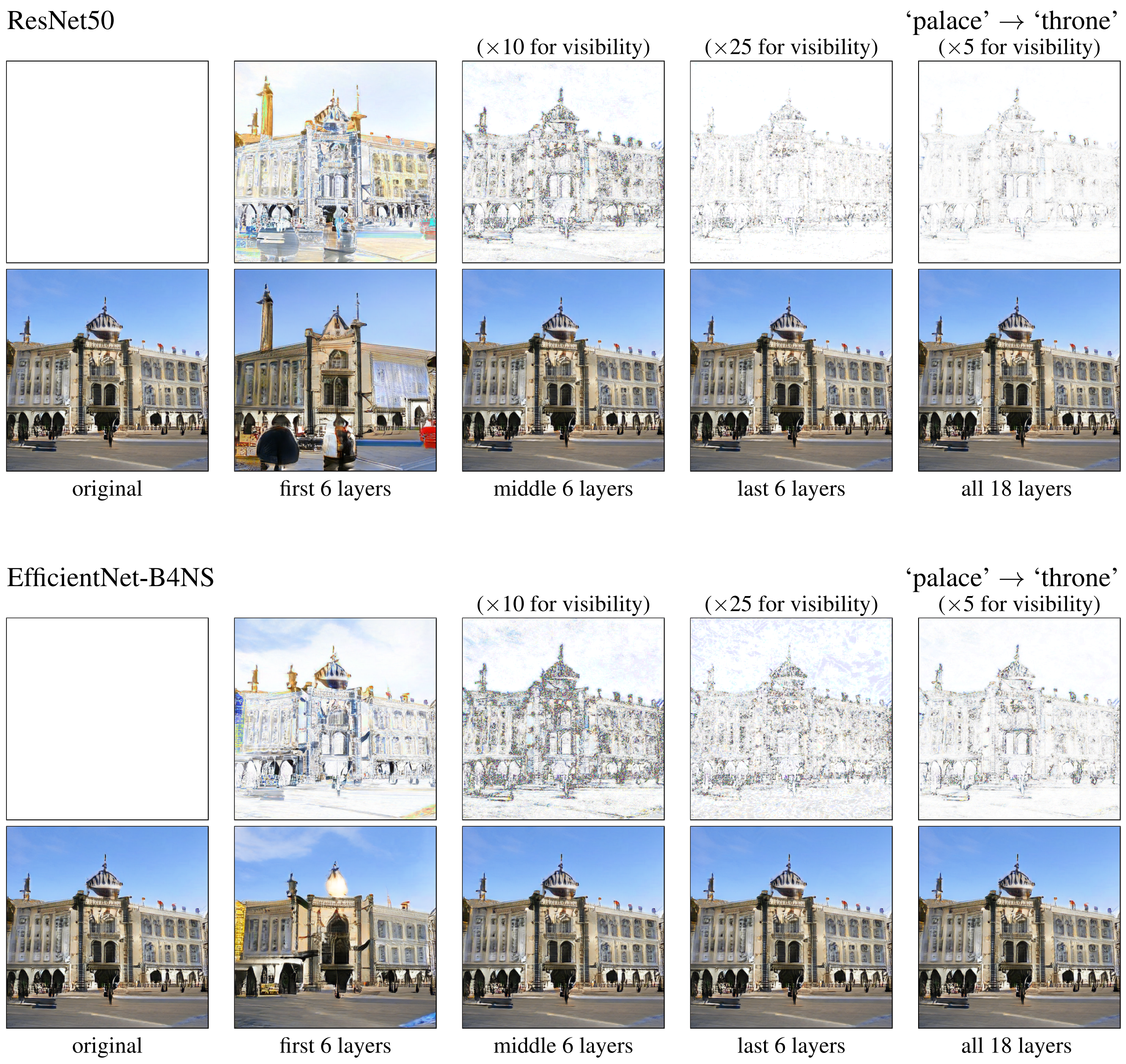

Figure 7: Examples of feature perturbations for the two standard classifiers. For each, the bottom row show the perturbed images for perturbations at different parts of the generator. The top row shows the pixel-wise difference between the original image and the perturbed image. Some of these have been scaled to be made more visible. The name of the classifier is shown in the top left, and in the top right, the original and target label.

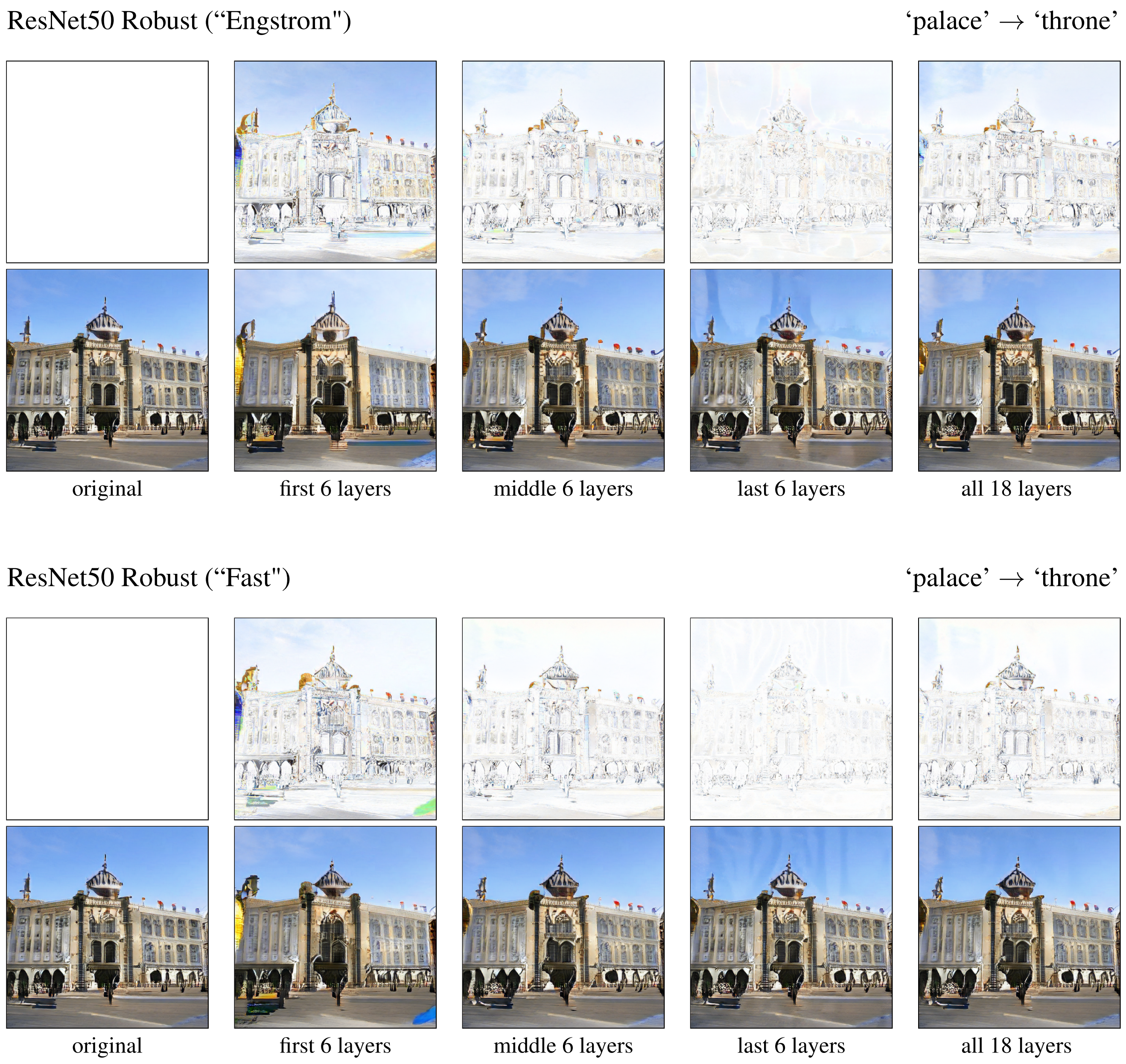

Figure 8: Examples of feature perturbations for the two pixel-robust classifiers. For each, the bottom row show the perturbed images for perturbations at different parts of the generator. The top row shows the pixel-wise difference between the original image and the perturbed image. The name of the classifier is shown in the top left, and in the top right, the original and target label.

E CelebA-HQ

Model details

Progressive GAN We use the pretrained CelebA-HQ 512×512 Progressive GAN from https://pytorch.org/hub/facebookresearch_pytorch-gan-zoo_pgan/. We simply perturb the activations after each 'scaleLayer' in this implementation. Note that unlike the other generative models we use, this is not a conditional model. That is, its only input is the random seed: you cannot specify that it generates an image with certain characteristics.

Table 5 details the layers of the Progressive GAN, and indicates which activations are perturbed.

Classifier CelebA is used primarily as benchmark for generative modelling, not discriminative classification. We could not find any pre-trained classifiers for the 40 binary attributes that the dataset is labelled with. In the absence of any suitable checkpoints, we simply used existing code to train the classifier we needed: https://github.com/aayushmnit/Deep_learning_explorations/tree/master/7_Facial_attributes_fastai_opencv. The resulting model obtains $> 90\%$ accuracy over the forty binary labels, certainly good enough for our purpose of demonstrating our method.

Experimental setup

CelebA is labelled with 40 binary attributes. It is very easy to flip the prediction of just one of these attribute predictions, but is difficult to flip all forty at once, if only because this is a forty-objective optimisation problem; multi-objective optimisation is notoriously challenging. As a sensible middle ground, we use our method to find context-sensitive perturbations that flip the sign of ten of the forty attributes, since $2^10 = 1024$, which is roughly the number of ImageNet classes. In particular, because the generator is not conditional, we cannot know which attribute predictions are correct. Our approach is therefore to perturb each image so that all the following labels are predicted positively: 'Bald', 'Blond hair', 'Eyeglasses', 'Goatee', 'Grey hair', 'Moustache', 'No beard', 'Wearing hat', 'Wearing necklace', and 'Wearing necktie'.

Since the generator has ten layers, we demonstrate the effects of perturbing the first four layers only, the next three layers, the final three layers, and all ten layers at once. The optimisation process required a modest amount of finetuning (a few hours of ad-hoc manual experimentation); as noted elsewhere, we perform *no* tuning of the layers selected to perturb at, or the relative scales of the perturbations at different neurons. We use a learning rate of 0.1. No epsilon bound is needed, since using this learning rate, the optimisation converges suitably without it. To help with the multi-objective optimisation, the logits are raised to the power of $\frac{1}{10}$, making the gradients steeper for the constraints not yet satisfied, and disincentivising further optimisation of the objectives already satisfied.

We did not have the resources to have an independent judge label these results, but we are satisfied by inspection that the results are similar to the ImageNet results, in that the large majority of perturbed images have not changed their original labels. Note that this claim is not about the photorealism of the generated images—which depends mainly on the generative model used—but on whether the perturbed images are not generally either unrecognisable as faces, or perturbed so that the predicted labels become accurate.

Results

We provide results in Figures 9, 10 and 11.

Please also refer to the separate Data Appendix to see animations showing the effect of gradually introducing the perturbations to the latent activations of the generator. These give the viewer a much clearer intuition for the nature of the changes being made to the images; using static comparisons alone can be difficult to interpret.

Table 5: CelebA-HQ convolutional generator architecture. Each row represents a layer. Each horizontal rule marks an activation tensor at which perturbations are performed.

Fully-Connected	(8192 units)
LeakyReLU	(Slope -0.2)
Reshape	(To batch of $512 \times 4 \times 4$ tensors)
2D Convolution	(3×3 kernel, stride 1, padding size 1, 512 feature maps)
LeakyReLU	(Slope -0.2)
Upscale	(To 8×8)
2D Convolution	(3×3 kernel, stride 1, padding size 1, 512 feature maps)
LeakyReLU	(Slope -0.2)
2D Convolution	(3×3 kernel, stride 1, padding size 1, 512 feature maps)
LeakyReLU	(Slope -0.2)
Upscale	(To 16×16)
2D Convolution	(3×3 kernel, stride 1, padding size 1, 512 feature maps)
LeakyReLU	(Slope -0.2)
2D Convolution	(3×3 kernel, stride 1, padding size 1, 512 feature maps)
LeakyReLU	(Slope -0.2)
Upscale	(To 32×32)
2D Convolution	(3×3 kernel, stride 1, padding size 1, 512 feature maps)
LeakyReLU	(Slope -0.2)
2D Convolution	(3×3 kernel, stride 1, padding size 1, 512 feature maps)
LeakyReLU	(Slope -0.2)
Upscale	(To 64×64)
2D Convolution	(3×3 kernel, stride 1, padding size 1, 256 feature maps)
LeakyReLU	(Slope -0.2)
2D Convolution	(3×3 kernel, stride 1, padding size 1, 256 feature maps)
LeakyReLU	(Slope -0.2)
Upscale	(To 128×128)
2D Convolution	(64×64 kernel, stride 1, padding size 1, 128 feature maps)
LeakyReLU	(Slope -0.2)
2D Convolution	(3×3 kernel, stride 1, padding size 1, 128 feature maps)
LeakyReLU	(Slope -0.2)
Upscale	(To 256×256)
2D Convolution	(3×3 kernel, stride 1, padding size 1, 64 feature maps)
LeakyReLU	(Slope -0.2)
2D Convolution	(3×3 kernel, stride 1, padding size 1, 64 feature maps)
LeakyReLU	(Slope -0.2)
Upscale	(To 512×512)
2D Convolution	(3×3 kernel, stride 1, padding size 1, 32 feature maps)
LeakyReLU	(Slope -0.2)
2D Convolution	(3×3 kernel, stride 1, padding size 1, 32 feature maps)
LeakyReLU	(Slope -0.2)
2D Convolution	(1×1 kernel, stride 1, 3 feature maps)

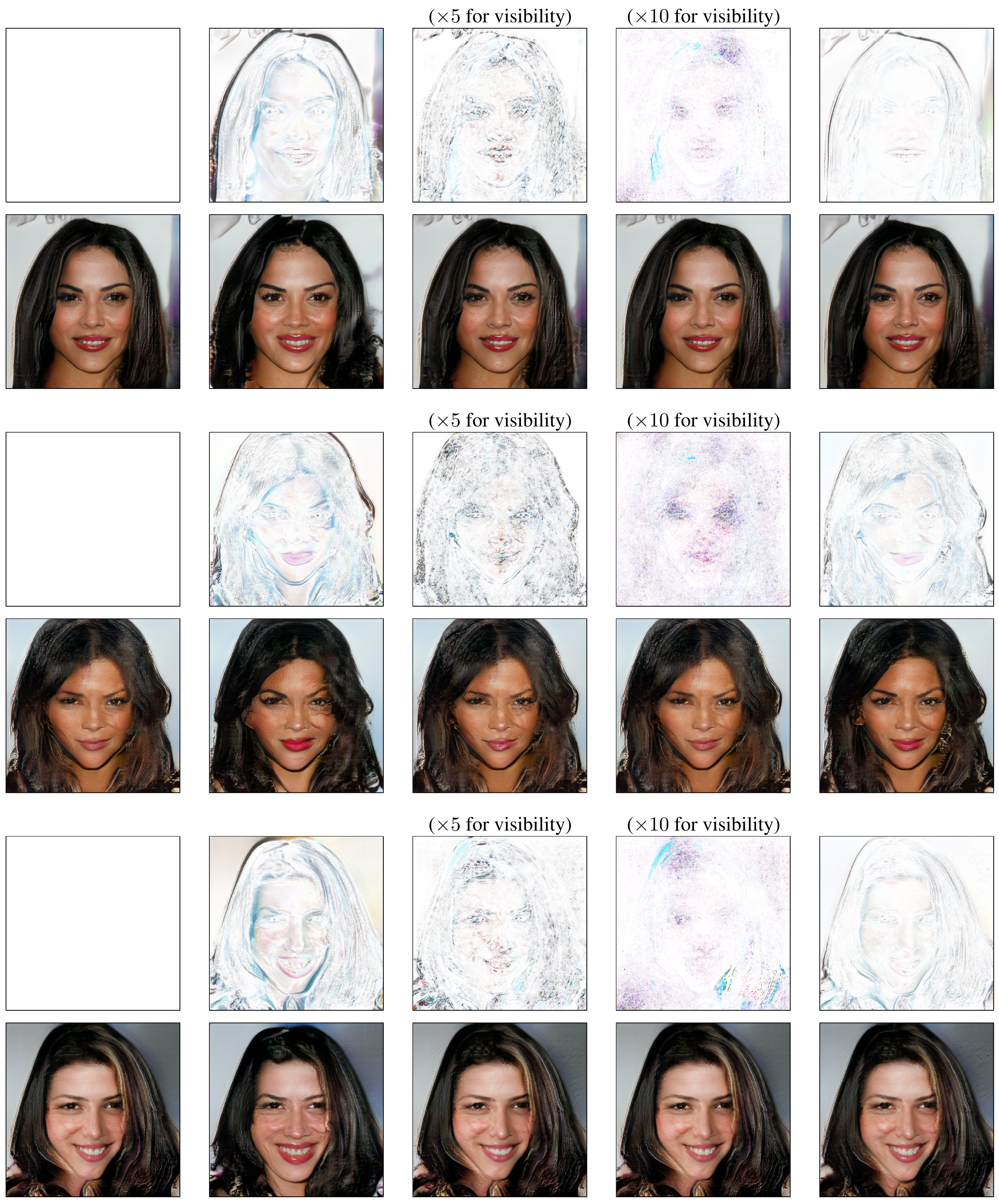

Figure 9: A random selection of context-sensitive feature perturbations at different granularities, as controlled by perturbing activations at the generator layers indicated under each image. Differences with the unperturbed image are shown above each perturbed image. Each perturbed image has the following labels predicted positively: ‘Bald’, ‘Blond hair’, ‘Eyeglasses’, ‘Goatee’, ‘Grey hair’, ‘Moustache’, ‘No beard’, ‘Wearing hat’, ‘Wearing necklace’, and ‘Wearing necktie’.

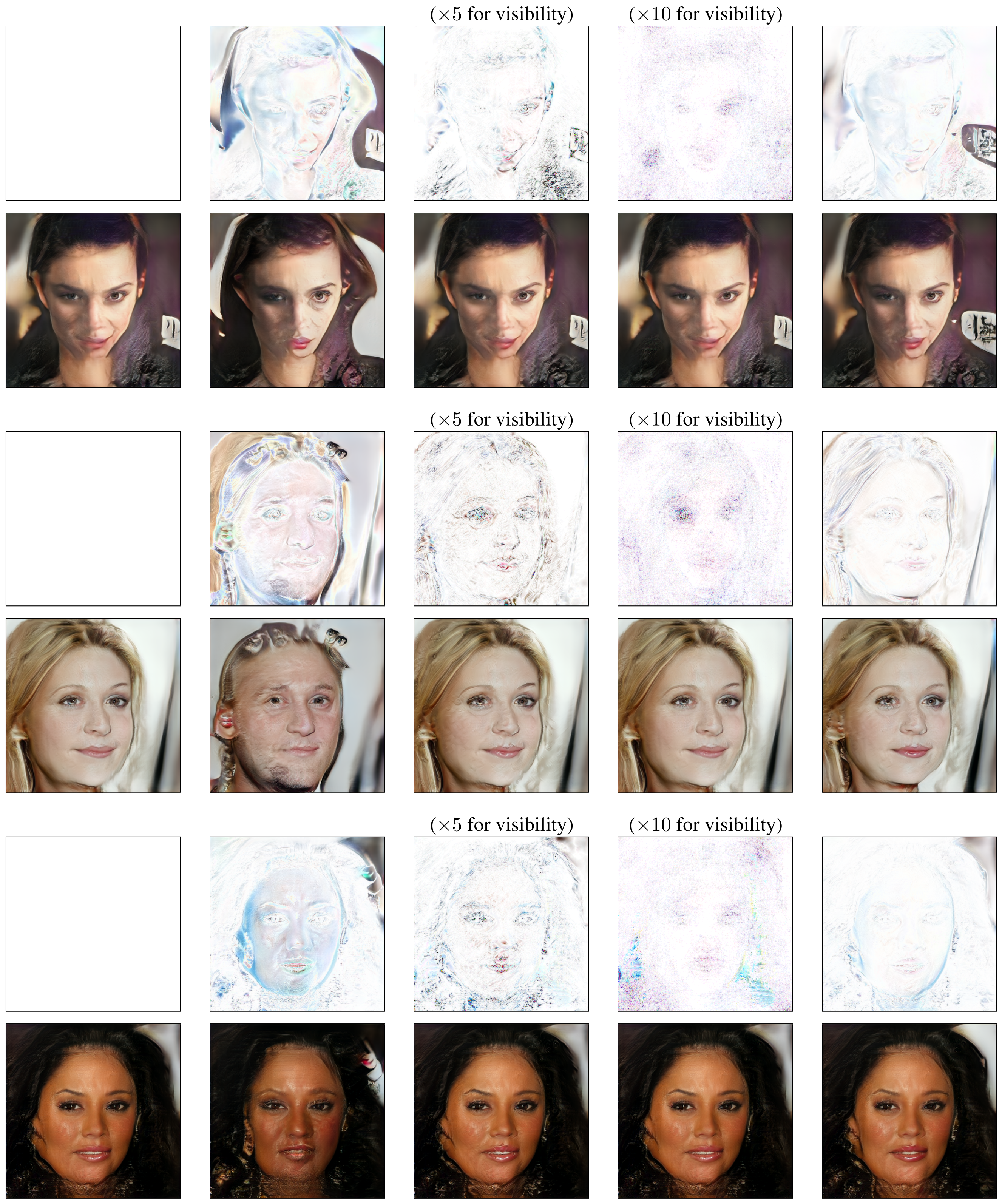

Figure 10: A random selection of context-sensitive feature perturbations at different granularities, as controlled by perturbing activations at the generator layers indicated under each image. Differences with the unperturbed image are shown above each perturbed image. Each perturbed image has the following labels predicted positively: ‘Bald’, ‘Blond hair’, ‘Eyeglasses’, ‘Goatee’, ‘Grey hair’, ‘Moustache’, ‘No beard’, ‘Wearing hat’, ‘Wearing necklace’, and ‘Wearing necktie’.

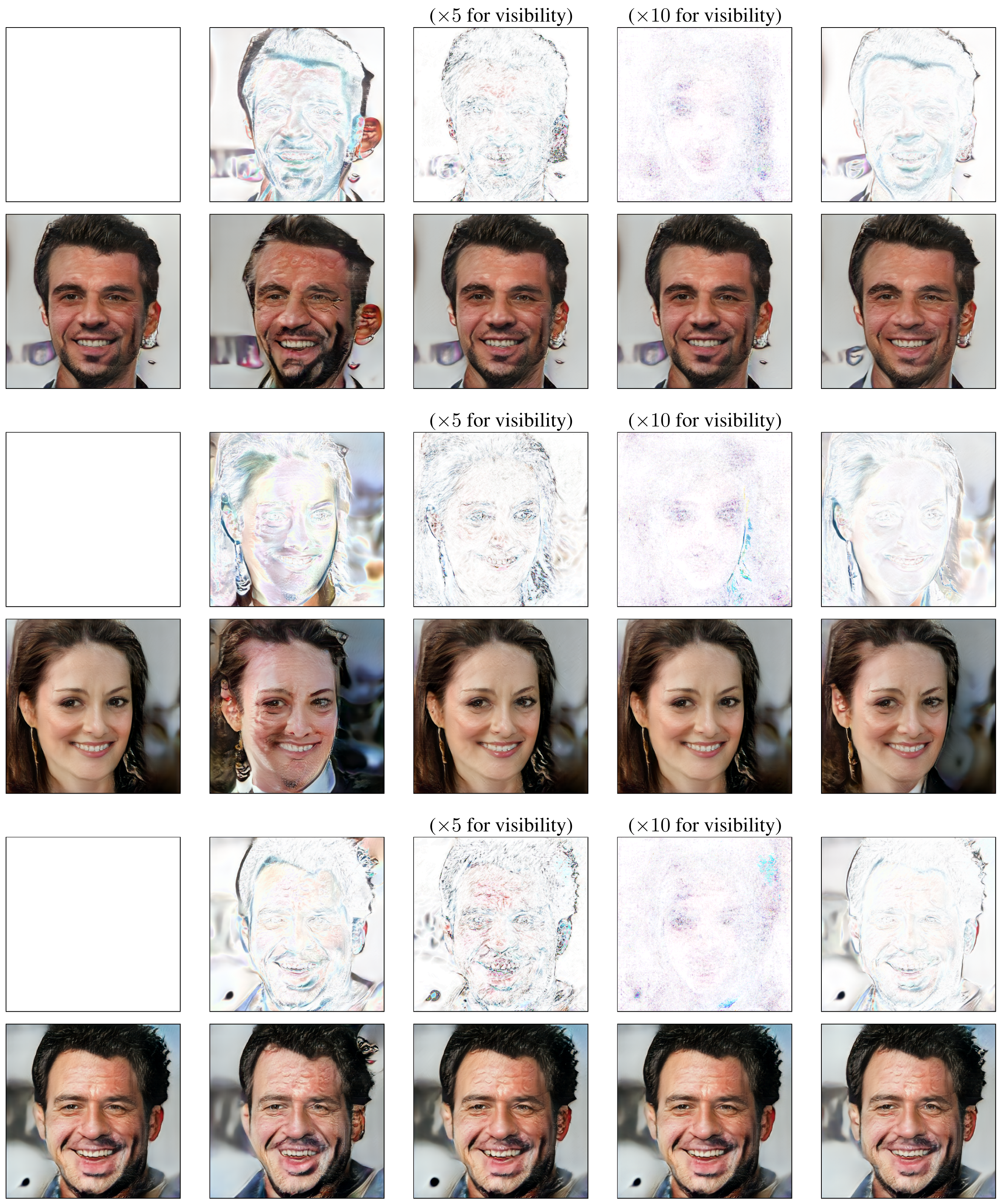

Figure 11: A random selection of context-sensitive feature perturbations at different granularities, as controlled by perturbing activations at the generator layers indicated under each image. Differences with the unperturbed image are shown above each perturbed image. Each perturbed image has the following labels predicted positively: ‘Bald’, ‘Blond hair’, ‘Eyeglasses’, ‘Goatee’, ‘Grey hair’, ‘Moustache’, ‘No beard’, ‘Wearing hat’, ‘Wearing necklace’, and ‘Wearing necktie’.

F MNIST

Model details

MNIST convolutional GAN For MNIST, we tried a range of generators and found that they all worked roughly as well as one another. For the experiments, we use a simple convolutional generator, inspired by the Deep Convolutional GAN (Radford, Metz, and Chintala 2016). Details are shown in Table 6. Inputs to the generator are drawn from a 128-dimensional standard Gaussian. The sigmoid output transformation ensures that pixels are in the range $[0, 1]$, as expected by the classifiers. We perform context-sensitive perturbations before ReLU layers, rather than after, to prevent ReLU output values from being perturbed to become negative, which would not have been encountered during training and so may not result in plausible images being generated since they are out-of-distribution for the rest of the generator. Note that perturbing before and after the sigmoid transformation has different effects because perturbations to values not close to 0 are diminished in magnitude if passed through the sigmoid function.

Classifiers We use two neural networks that classify MNIST. One is a simple standard classifier with two convolutional layers and three fully-connected layers, trained to give an accuracy over 99%. The other is an LeNet5 classifier adversarially trained against l_2-norm bounded perturbations for $\epsilon = 0.3$. This was trained using the AdverTorch library (Ding, Wang, and Jin 2019). It has a standard accuracy of 98%, reduced to 95% by an l_2-norm bounded attack with $\epsilon = 0.3$.

Experimental setup

We find context-sensitive feature perturbations as described for ImageNet in Appendix B, with a few differences. First, since the generator is much smaller, we divide it nearly in half, comparing the effect of perturbing the activation values at first four layers only with the effect of perturbing at the last four layers only. Second, because MNIST (and the generator) is much smaller, so are the perturbation magnitudes required. So the learning rate is reduced to 0.004, the we start with an initial perturbation magnitude constraint of 0.1, and this is gradually relaxed after each optimisation step by increasing this upper bound by 0.001. The procedure for collecting human judgements is as described in Appendix B.

Results and discussion

Figure 12 shows the robustness of the two classifiers to the two kinds of context-sensitive perturbation. We can see from Figure 12b that the classifier trained to be robust to pixel-space perturbations is indeed more robust than the standard classifier, with its considerably shallower slope indicating that a bigger perturbation magnitude is required to the finer-grained features encoded in the last four layers of the generator.

Conversely, Figure 12a gives an almost-identical shape for both classifiers, indicating that adversarial training against pixel-space perturbations does not confer any robustness to the coarse-grained feature perturbations being evaluated here.

Table 6: MNIST convolutional generator architecture. Each row represents a layer. Each horizontal rule marks an activation tensor at which perturbations are performed.

Fully-Connected	(64 units)
ReLU	
Transposed Convolution	(5×5 kernel, 2×2 stride, 32 feature maps)
Batch Normalisation	
Leaky ReLU	(Slope -0.2)
Dropout	($p = 0.35$)
Transposed Convolution	(5×5 kernel, 2×2 stride, 8 feature maps)
Batch Normalisation	
Leaky ReLU	(Slope -0.2)
Dropout	($p = 0.35$)
Transposed Convolution	(5×5 kernel, 2×2 stride, 4 feature maps)
Batch Normalisation	
Leaky ReLU	(Slope -0.2)
Dropout	($p = 0.35$)
Fully-Connected	(784 units)
Sigmoid	($\tanh$ used during training)

This has an interesting relationship with our main finding, that adversarial training against pixel-space perturbations seriously harms robustness to high-level context-sensitive features perturbations on ImageNet. The difference can likely be best explained by the great difference in datasets. The dimensionality of ImageNet is over $1000\times$ greater, and the high-level feature space of MNIST is trivially small in comparison. The result of this is that in some loose sense, there is a smaller 'gap' between the highest- and lowest-granularity features encoded in the generator; put another way, there is a much less rich space of coarse-grained context-sensitive features that a classifier must be robust to on MNIST.

Whether this is the correct intuition, the implications of our finding remains clear: even on the very simplest datasets, robustness to fine-grained features completely fails to generalise to coarser-grained features. If we are to obtain classifiers that we can trust to generalise under modest distributional shifts, there is still far to go.

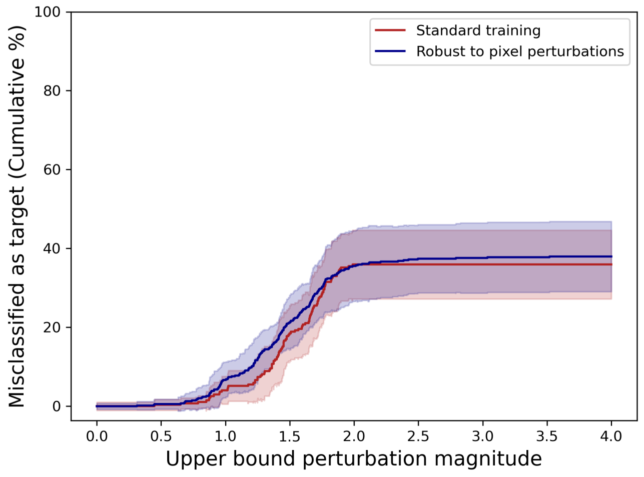

(a) Generator activations perturbed at first 4 layers only.

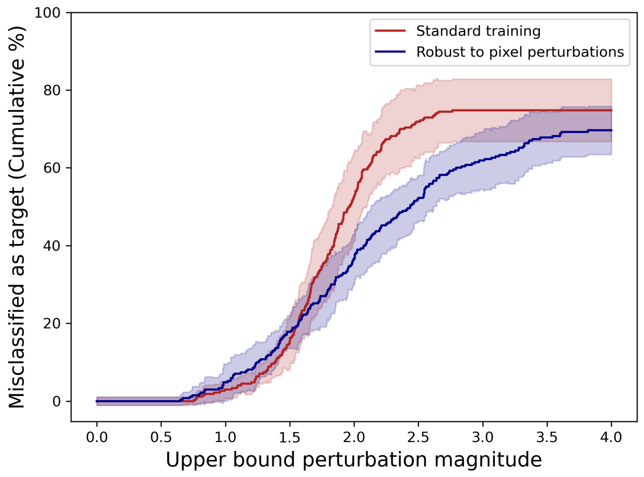

(b) Generator activations perturbed at last 4 layers only.

Figure 12: Graphs showing how the proportion of perturbations that induce the targeted misclassification increases with perturbation magnitude. These should be interpreted in the same way as Figure 4. The solid lines exclude the perturbed images for which a human judges that the perturbation does not change the true label of the image; the dotted lines, for reference, include these.

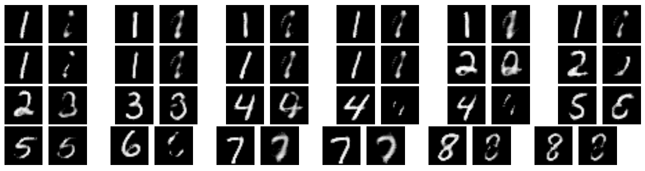

Figure 13: Random sample of context-sensitive perturbations targeting label 0. Only the first four layers of generator activations are perturbed, and the classifier is trained using a standard training procedure. In each pair, the perturbed image is to the right of the unperturbed image.

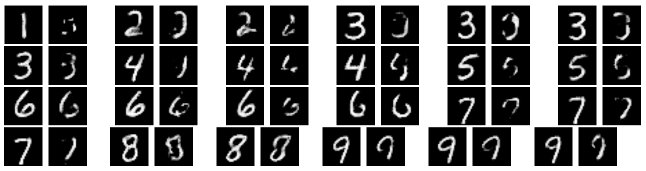

Figure 14: Random sample of context-sensitive perturbations targeting label 0. Only the first four layers of generator activations are perturbed, and the classifier is trained using adversarial training. In each pair, the perturbed image is to the right of the unperturbed image.

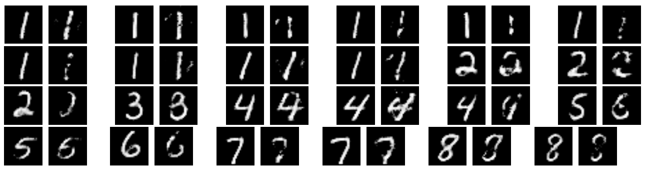

Figure 15: Random sample of context-sensitive perturbations targeting label 0. Only the last four layers of generator activations are perturbed, and the classifier is trained using a standard training procedure. In each pair, the perturbed image is to the right of the unperturbed image.

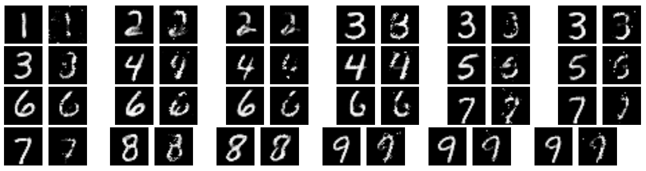

Figure 16: Random sample of context-sensitive perturbations targeting label 0. Only the last four layers of generator activations are perturbed, and the classifier is trained using adversarial training. In each pair, the perturbed image is to the right of the unperturbed image.